CrossMark

Synthesis of graphitic carbon nitride via direct polymerization using different precursors and its application in lithium–sulfur batteries

Shanshan Yao[1] · Sikang Xue[1] · Sihuang Peng[1] · Ruiduo Guo[1] · Zongzhen Wu[1] · Xiangqian Shen[1,2] · Tianbao Li[2] · Li Wang[2]

Abstract

The graphitic carbon nitride (g-C_3N_4) materials were prepared via direct polymerization of urea, melamine, thiourea, and dicyandiamide at the same conditions, respectively. The samples were tested by various characterization tools, so that to study the influences of precursors on the physical and electrochemical properties of g-C_3N_4. The results showed that the as-prepared U-CN (from urea), M-CN (from melamine), T-CN (from thiourea), and D-CN (from dicyandiamide) exhibited significantly different microstructures. The synthesized g-C_3N_4 powders were used as sulfur matrixes for lithium–sulfur batteries. The electrochemical properties revealed that urea-derived C_3N_4 showed the highest initial capacity of 1207 mAh g^{-1}. Furthermore, it possesses excellent cycling stability for 500 cycles and remains capacity of 517 mAh g^{-1} at 0.37 mA cm^{-2}. This work could provide a new perspective for the selection of proper precursors and the in-depth study of the electrochemical behaviors of the microstructure of g-C_3N_4.

1 Introduction

Lithium ion batteries have revolutionized the portable electronic devices, which could not meet the requirements for large-scale grid applications and electric vehicles [1]. The current lithium ion battery technology based on transition-metal oxide cathodes and nanoengineered carbon anode has limited energy storage capacity [2–6]. Lithium–sulfur batteries (LSB) have an overwhelming advantage in energy density, with a theoretical value of about 2600 Wh kg^{-1} calculated on the basis of the lithium anode and the sulfur cathode, and is up to several times greater than that of traditional lithium ion batteries [7]. However, the widespread usage of LSB is limited by a few defects such as poor coulombic efficiency, fast fading of specific discharge capacity, irreversible loss of active material, and poor cycle life [8, 9]. The above issues may be attributed to the insulation of sulfur and dissolved intermediate lithium polysulfides (Li_2S_x, $4 \leq x \leq 8$) into electrolyte during charge–discharged process, which is the culprit of the shuttle effect [10–12].

To address the above stated problems, widespread efforts have dedicated, including the design new cell structures [13], electrolyte [14], passivation of anode [15], and novel technology to encapsulate sulfur in cathode [16]. Among these, the current research tends to wrap sulfur in the porous host. Mesoporous/microporous carbon [17], carbon nanofibers [18], and graphene [19] have been applied as sulfur matrixes in cathode. Nevertheless, microstructure materials like these with varying pore size distribution could retain polysulfides in the porous structure via a physical way. This combination of carbon matrix and polysulfides is neither durable nor enough. Polysulfides were absorbed by a chemical way which was investigated widely in recent years, such as the nitrogen atoms in carbon materials [20], the multifunction groups [21], and other polar compounds [22]. There are three kinds of forms of nitrogen atoms in nitrogen (N)-doped carbon matrixes, which conclude pyridinic N, pyrrolic N, and quaternary N [23, 24]. These previous results proved that the nitrogen in doped states also possesses strong

✉ Shanshan Yao
  yaosshan@ujs.edu.cn

[1] Institute for Advanced Materials, College of Materials Science and Engineering, Jiangsu University, Zhenjiang 212313, People's Republic of China

[2] Hunan Engineering Laboratory of Power Battery Cathode Materials, Changsha Research Institute of Mining and Metallurgy, Changsha 410012, People's Republic of China

chemical bond with polysulfides. Moreover, these nitrogen modified carbon allows the uniform distribution of active substances and creates more active sites on the surface of carbon hosts [25].

Graphitic carbon nitride (g-C_3N_4) nanosheets are a representative graphitic-like two-dimensional (2D) layered material, weaker van der Waals force between layers ensures a 2D-layered structure and connected with the amino group of each layer to form a tri-s-triazine unit structure [26, 27]. In practically, g-C_3N_4 can be prepared by the pyrolysis of various nitrogen-rich precursors. For example, g-C_3N_4 was synthesized with 2-amino-4, 6-dichlorotriazine by Zhang et al. in a suitable condition [28]. Xu et al. prepared g-C_3N_4 by directly heating dicyandiamide first at 350 °C for 2 h and then 550 °C for another 2 h, respectively [29]. Chuang et al. obtained g-C_3N_4 from urea at 550 °C for 3 h [30]. Depending on reaction conditions, g-C_3N_4 with different degrees of condensation and properties was obtained [31, 32]. So far, little information is known about the effects of different precursors on physical and chemical properties of g-C_3N_4 under the same conditions, such as surface area, pore volume, morphology, and electrochemical behaviors.

In the present work, considering the fact the g-C_3N_4 samples prepared from urea, melamine, thiourea, and dicyandiamide separately have different physicochemical properties, the molecular composite precursor of urea, melamine, thiourea and dicyandiamide were treated simultaneously under the same thermal condition. Various characterization tools were utilized to analyze the influences of precursor on the physicochemical properties of g-C_3N_4. The g-C_3N_4 powders were used as sulfur matrix for LSB. These results showed that the precursors have considerable impact on the electrochemical properties of g-C_3N_4.

2 Experiments

2.1 Preparation of g-C_3N_4 and sulfur/g-C_3N_4 electrodes

High nitrogen-level compounds, including urea, melamine, thiourea, and dicyandiamide, were selected as precursors and g-C_3N_4 powders were obtained by polymerization process. A weighed precursor was placed in differently labeled alumina crucibles and calcined at 550 °C for 4 h in muffle furnace. When the furnace temperature dropped to room temperature, the as-prepared g-C_3N_4 were collected and used as such for further studies. In practical, the different g-C_3N_4 prepared from urea, melamine, thiourea and dicyandiamide were labeled as U-CN, M-CN, T-CN and D-CN. Figure S1 in Supporting Information illustrates the procedure for obtaining bulk g-C_3N_4.

Then, the U-CN was mixed with sublimed sulfur by ball milling and the mass ratio is 3:7. The mixture was then transferred to a vacuum drying oven and dried overnight at 60 °C to remove the moisture present in the powder. The dried powder material is sealed in a stainless steel reactor with PTFE liner and kept at 155 °C for half a day to obtain S/U-CN composite. The slurry of S/U-CN composite cathode was prepared from a mixture of the as-fabricated S/U-CN composite materials, conductive carbon black, and binder using mass ratio of 7:2:1. Using carbon-coated aluminum foil as the current collector and coating the above slurry on the surface uniformly, cathode should be also dried at the particular condition which is same with condition of mixture after ball milling. Finally, the S/U-CN cathodes with 1.13 cm^2 have approximately 2.2 mg cm^{-2} sulfur loading. For comparative analysis, S/M-CN, S/T-CN, S/D-CN, and pure sulfur electrodes were also prepared following the procedure described above. The sulfur/g-C_3N_4 electrodes are schematically exhibited in Figure S2 of Supporting Information.

2.2 Materials characterization

XRD (Rigaku D/Max 2500PC) was utilized to analysis the phase analysis of materials by diffraction with using Cu Ka radiation. The specific surface area measurements of samples were carried out via BET analysis using a pore size distribution analyzer (NOVA 2000e). The morphology of the prepared samples was demonstrated by scanning electron microscopy (SEM, JSM-7001F). The morphologies and structures of the samples were further understood by high-resolution transmission electron microscopy (HRTEM, Tecnai G2 F30) at an acceleration voltage of 200 kV.

2.3 Electrochemical measurement

The electrochemical behavior of the four samples was measured using a CR2032-type coin cells system. Lithium metal foil and celgard 2400 polypropylene film were selected as anode and the separator. The electrolyte solvent is 1, 2-dimethoxyethane (DME) and 1,3-dioxolane (DOL) at a volume ratio of 1:1, the solute is 1 M lithium bis(trifluoromethanesulfone)imide (LiTFSI) and 0.1M lithium nitrate. In addition, electrolyte is added about 100 μL in each cell. The cells within S/CN composite cathodes were tested cycle performance at 0.37 mA cm^{-2} (1C = 1675 mA g^{-1}) by a CT2001A cell test equipment (LAND model, Wuhan RAMBO testing equipment, Co., Ltd) from 1.7 to 2.8 V (vs. Li/Li$^+$). A scanning speed of 0.1 mV s^{-1} was selected in cyclic voltammetry (CV) measurements at the same voltage ranging with cycle performance. The EIS measurements in the 10 mHz ≤ frequency ≤ 100.0 kHz were recorded using a VMP2 electrochemical workstation (DHS

Instruments Co., Ltd.) at an alternating current (AC) voltage of 10 mV.

3 Results and discussion

3.1 Characterization of as-prepared g-C₃N₄ with different precursor

The XRD patters (Fig. 1a) of the specimens prepared from urea, melamine, thiourea and dicyandiamide can be indexed to g-C₃N₄, masked as U-CN, M-CN, T-CN and D-CN, respectively. The strongest interplanar stacking peaks of the conjugated aromatic systems at around 27.4° are indexed to graphitic materials as the (002) peak. The low intensity peak at 12.9° can be linked to the in-plane structural repeat

motif of the (100) tri-s-triazine unit [33, 34]. Moreover, the presence of two characteristic peaks in Fig. 1a indicates that its basic structure was fully preserved in all g-C₃N₄ samples. In addition, the XRD patters of the S/g-C₃N₄ composites are demonstrated in Fig. 1b, which proved that the sublimated sulfur in the S/g-C₃N₄ composite is a kind of the orthorhombic sulfur particles phases (JCPDS: 08-0247).

As shown in Fig. 2a, the pore volumes of M-CN with $0.02 \text{ cm}^3 \text{ g}^{-1}$ and $0.03 \text{ cm}^3 \text{ g}^{-1}$ of D-CN are clearly lower than that $0.32 \text{ cm}^3 \text{ g}^{-1}$ of U-CN and $0.12 \text{ cm}^3 \text{ g}^{-1}$ of T-CN. The BET analysis significantly illustrates that the heteroatoms of oxygen and sulfur play a crucial role in enhancing the pore volumes of g-C₃N₄ during the condensation. The formation of carbon dioxide and hydrogen sulfide, release of ammonia, and generation of additional water vapor during the pyrolysis of urea and thiourea favor the expansion
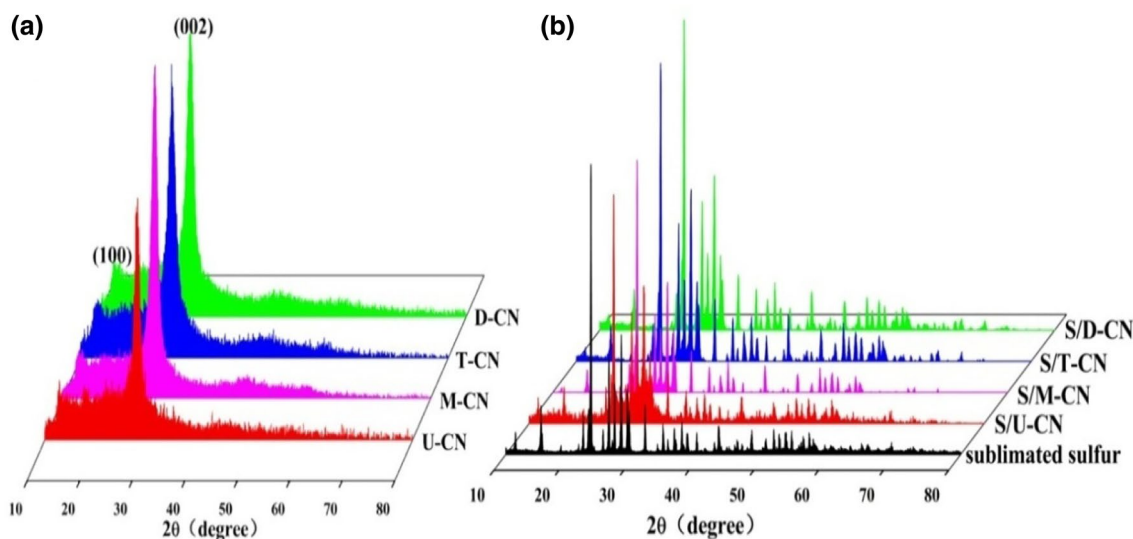

Fig. 1 Powder XRD patterns of **a** U-CN, M-CN, T-CN, D-CN specimens and **b** S/U-CN, S/M-CN, S/T-CN, S/D-CN and sublimated sulfur
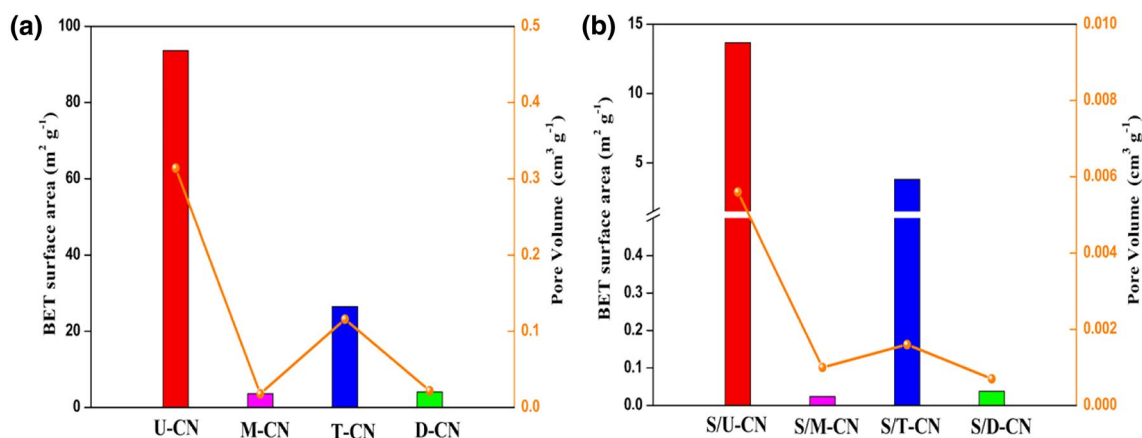

Fig. 2 BET surface areas and pore volumes of **a** U-CN, M-CN, T-CN; D-CN specimens and **b** S/U-CN, S/M-CN, S/T-CN, S/D-CN composites

of the packing layers and porous structure. Meanwhile, the porous structure of urea-derived g-C_3N_4 with the high BET surface areas was expected to enhance electrochemical properties [35–37]. Compared with pure CN powders, the specific surface areas and pore volumes of the obtained S/CN hybrids decrease drastically (Fig. 2b), suggesting that the porous structures of CN matrices are all occupied by the incorporated sulfur particles.

The SEM images of the as-prepared U-CN, M-CN, T-CN and D-CN are demonstrated in Figure S3. Obviously, the porous structure of CN consists of thin CN nanosheets with porosity, which can also be confirmed in Fig. 3. The morphological features as seen by TEM, however, revealed significant differences. TEM image of U-CN in Fig. 3a displayed thinner sheets crinkly paper-folded and the M-CN in Fig. 3b can be characterized as an agglomerate of flat sheets, but due to the layered structure of the CN, the resulting
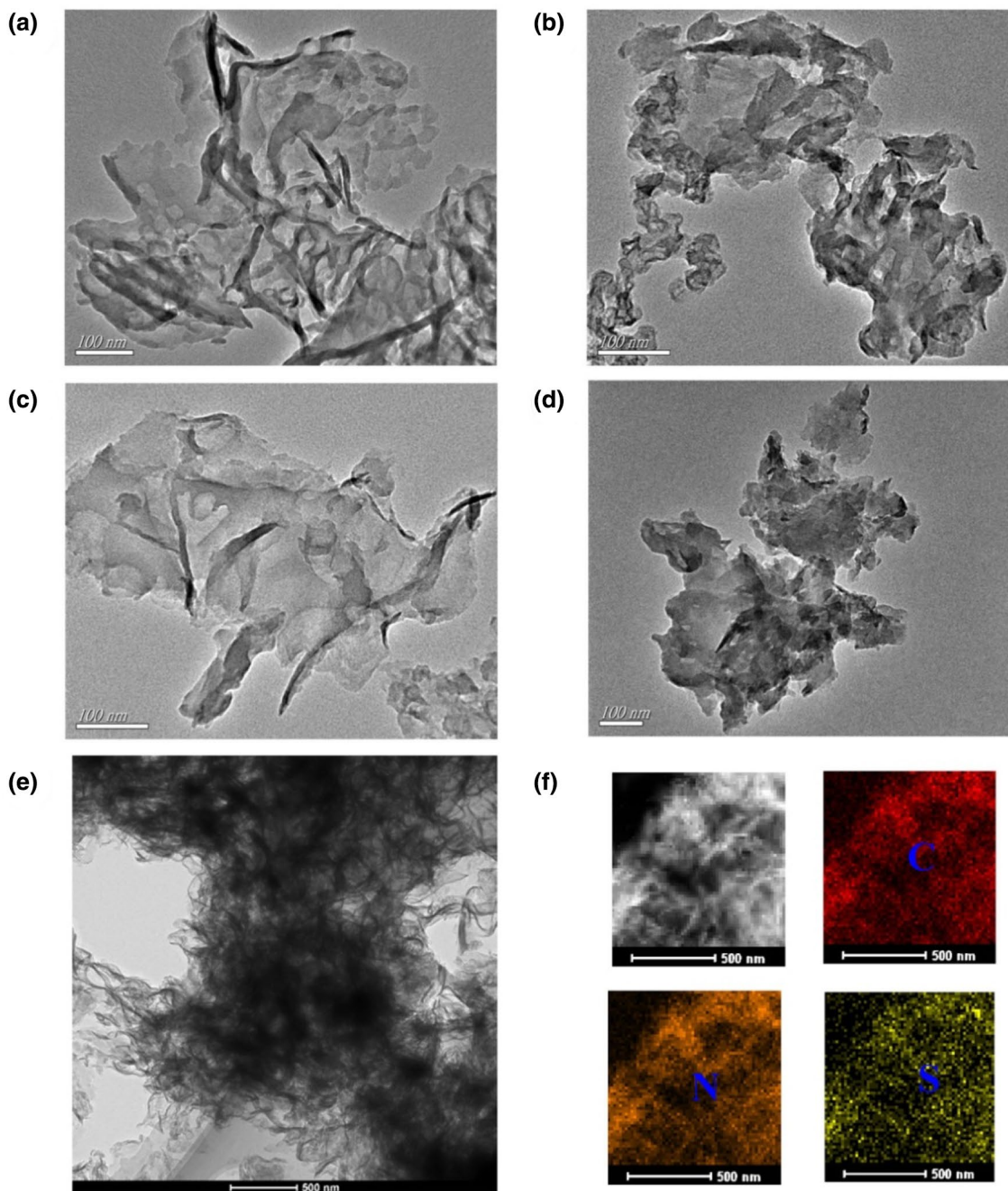

Fig. 3 TEM images of **a** U-CN, **b** M-CN, **c** T-CN and **d** D-CN; TEM image (**e**) and elemental mapping (**f**) of S/U-CN

aggregates have a smooth surface. A TEM image of T-CN in Fig. 3c demonstrates large thick film curled sheets. The D-CN in Fig. 3d revealed layered platelet-like morphology. The TEM images, respectively, show unique morphological and structure differences between all the CN derived from different precursors. The presence of hetero-atoms oxygen and sulfur led to different degrees of folding of U-CN and T-CN, respectively [34]. These condensation pathways are longer than the condensation pathways of M-CN and D-CN, which results in multiple exfoliations of the layer and the formation of sheets that fold into different degrees. Meanwhile, M-CN and D-CN constrain the formation of planar aggregates [38].

TEM image of S/U-CN (Fig. 3e) clearly shows that the pores of CN are filled with sulfur. The elemental mapping analysis was also carried out to give insight to the composing of S/U-CN and the uniformity of sulfur in porous U-CN. The element mapping images (Fig. 3f) of porous S/CN proves the uniform distribution of sulfur in the porous U-CN.

3.2 Electrochemical performance of S/g-C$_3$N$_4$ electrodes

The electrochemical behavior of pure sulfur and S/g-C$_3$N$_4$ composites cathodes were tested by cyclic voltammetry at first cycle, as shown in Fig. 4, of which testing ranging is from 1.7 to 2.8 V with 0.1 mV s^{-1}. There are three redox peaks in the testing results, which coincides with the two cathodic and oxidation peaks of the classic features of lithium–sulfur batteries. Two typical reduction peaks near 2.25 and 1.95 V correspond to the process of sulfur particles changing to long-chain dissolved polysulfides and the conversion of the insoluble Li$_2$S/Li$_2$S$_2$ from low-order

polysulfides, respectively [39]. Here, compared with the pure sulfur and S/CN cathodes (Fig. 4a), the S/U-CN composite cathode demonstrates the lowest voltage hysteresis in electrochemical polarization (ΔV), showing that S/U-CN composite cathode has more full electrochemical redox reaction and low internal resistance in LSB. In addition, the magnified the reduction peak around 1.95 V is shown in Fig. 4b. Compared with the reduction peak of pure sulfur electrode, the red shift of reduction peak can be detected, which may prove the g-C$_3$N$_4$ loading, increasing the kinetics of electrochemical reactions in cell.

Figure 5a shows the cycling performance of pure sulfur and S/CN composites electrodes between 1.7 and 2.8 V. The pure sulfur cathode has the lowest initial specific discharge capacity of 567 mAh g^{-1} and only remained specific discharge capacity of 157 mAh g^{-1} after 200 cycles at 0.37 mA cm^{-2}. In contrast, the cycle performance of the cells with S/CN composite cathodes was clearly improved. The S/U-CN, S/T-CN, S/D-CN and S/M-CN composites electrodes deliver the initial specific discharge capacity of 1207, 1080, 816, and 767 mAh g^{-1}, and separately maintained about 517, 375, 282, and 243 mAh g^{-1} after 500 cycles at the same current. Meanwhile, the rate performances of the cells with S/CN composite cathodes at different current density which are from 0.37 to 1.85 mA cm^{-2} are also analyzed. As shown in Fig. 5b, it is clearly exhibited that the rate performance of S/U-CN composite cathode is much better than other S/CN composites cathodes and pure sulfur cathodes. Even at 1.85 mA cm^{-2}, a reversible specific discharge capacity of 560 mAh g^{-1} was also achieved for the S/U-CN cathodes. These results show that as-prepared g-C$_3$N$_4$ in which different nitrogen-rich precursors could truly affect its electrochemical behavior of LSB.
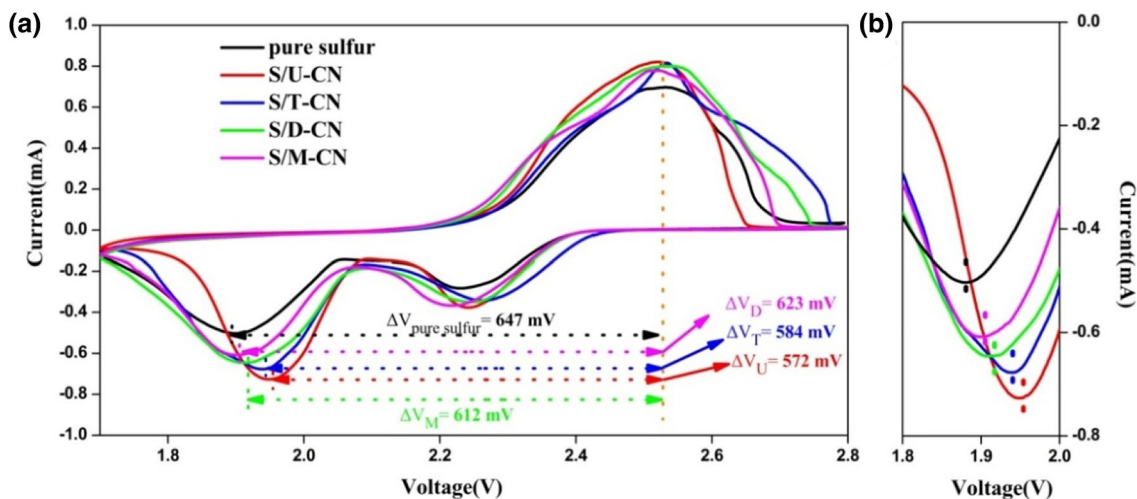

Fig. 4 Full (**a**) and magnified (**b**) cyclic voltammogram profiles of the S/U-CN, S/M-CN, S/T-CN, S/D-CN and pure sulfur electrodes
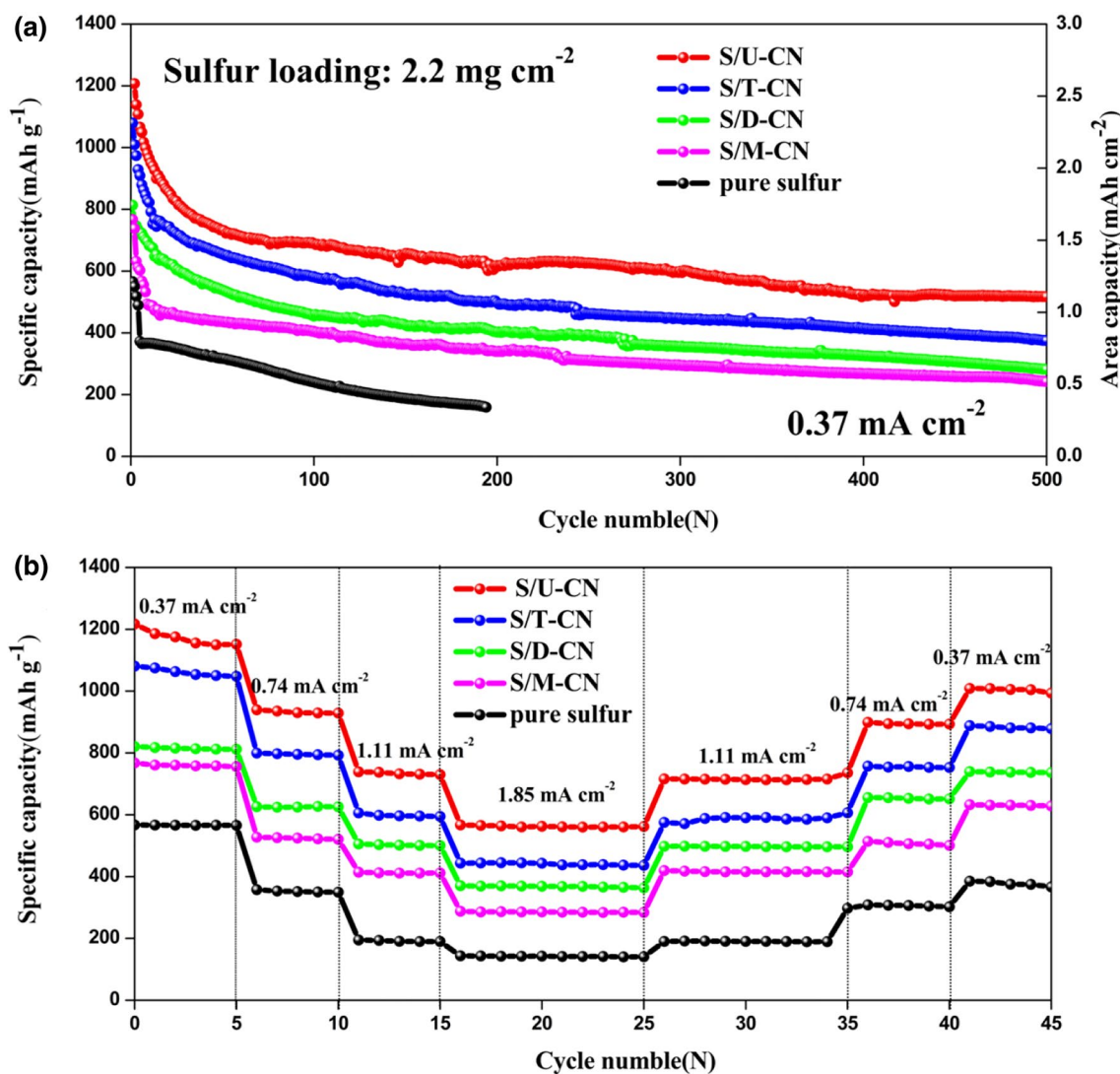
Fig. 5 a Cycle performances and **b** rate behaviors of S/U-CN, S/M-CN, S/T-CN, S/D-CN and pure sulfur electrodes

Electrochemical impedance spectroscopy (EIS) measurement of a pure sulfur cathode and S/U-CN, S/T-CN, S/M-CN, and S/D-CN composite cathodes are also performed in Fig. 6a. The dates of EIS consist of the high-frequency region is semi-circular and the straight line is represented low-frequency region, which is related to the electron transfer resistance and Li⁺ diffusion within the cathode. The equivalent circuit schematic is shown in Fig. 6b. R_1 shows the sum of interfacial resistances, including the electrodes and separators after the electrolyte is immersed. The charge transfer resistance in cell was reflected by R_2. W_{01} in the equivalent circuit diagram indicates the Warburg resistance caused by the diffusion of Li⁺ to the anode within the cathode [40]. Table 1 shows the related resistance dates of the five cathodes. Apparently, the S/U-CN cathode possesses the lowest charge transfer resistance than other S/CN composite cathodes and pure sulfur cathode, demonstrating a more

comfortable charge transfer environment between active materials and U-CN.

To further prove the impact of mobility coefficient of lithium ion, we initially calculated the Warburg diffusion coefficient σ which is obtained using Eq. (1) as follows [41, 42]:

$$Z_{re} = R_1 + R_2 + \sigma\omega^{-0.5}, \tag{1}$$

where both R_1 and R_2 are kinetics parameters independent of frequency. Therefore, values of σ which are displayed in Fig. 6c represent the slopes for the plots of Z_{re} vs. the reciprocal square root of the lower angular frequencies ($\omega^{-0.5}$). Then, the diffusion coefficient values of the lithium ions (D_{Li}^+) for the pure sulfur cathode and S/U-CN, S/T-CN, S/M-CN, S/D-CN composites cathodes were calculated by Eq. (2) and are also listed in Table 1 [43]:

$$Z_{re} = 0.5\left(\frac{RT}{AF^2\sigma C}\right)^2. \tag{2}$$
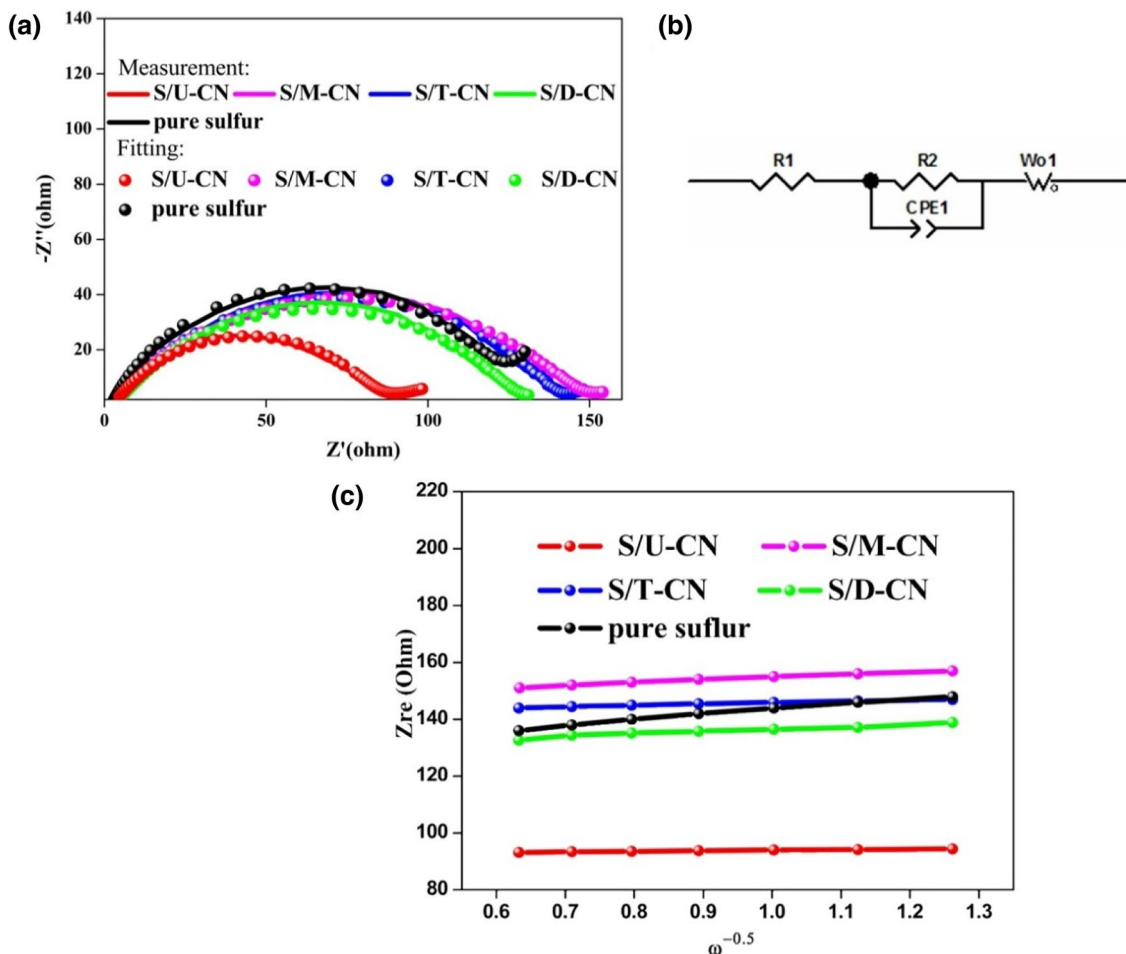
(a)

(b)

(c)

Fig. 6 **a** EIS of the as-prepared CN by different precursors with sulfur cathodes and a pure sulfur cathode, **b** schematic diagram of equivalent circuit, **c** the relationship between Z_{re} and $\omega^{-0.5}$ at low frequencies of S/CN composite cathodes

Table 1 Impedance parameters of the cathodes

| Cathodes	R_1 (Ω)	R_2 (Ω)	σ (Ω s$^{-1/2}$)	D_{Li+} (cm^2 s^{-1})
S/U-CN	2.1	92.1	1.9	6.4×10^{-9}
S/M-CN	6.1	139.4	9.5	2.5×10^{-10}
S/T-CN	3.2	135.6	4.8	1.0×10^{-9}
S/D-CN	3.9	117.9	7.8	3.8×10^{-10}
Pure sulfur	4.5	130.2	19.1	6.3×10^{-11}

In the above formula, F ($= 9.65 \times 10^4$ C mol^{-1}) is the Faraday's constant, and C ($= 1.1 \times 10^{-3}$ mol cm^{-3}) is the molar concentration of Li$^+$ ions, R ($= 8.314$ J mol^{-1} K^{-1}) is the gas constant, T ($= 298.5$ K) is the room temperature and A ($= 1.13$ cm^{-2}) is the area of the electrode surface. Similarly, the σ of S/U-CN is lower than that other S/CN composites and pure sulfur cathode, demonstrating the better diffusion environment. This good diffusion environment can be further enhanced by effective adsorption of urea-derived

g-C$_3$N$_4$ for the lithium polysulfides, due to its highest specific area, largest pore volume and crinkly paper-folded thinner sheets. Thus, all of these electrochemical measurements show that the g-C$_3$N$_4$ materials applied to different microstructures of exhibit different electrochemical properties as sulfur matrix in lithium–sulfur batteries.

To illustrate the effects of U-CN in a lithium–sulfur battery from the cycled cathode, the cell was transferred to a glove box and disassembled after a specified cycle test. The cycled S/U-CN composite cathode was repeatedly cleaned with anhydrous tetrahydrofuran (THF) and dried at 60 °C for overnight in a vacuum environment remove electrolyte before TEM testing.

The sulfur or lithium polysulfides adsorption of U-CN nanosheet can still be observed, as shown in Fig. 7. However, due to the high vacuum and high voltage HRTEM testing environment and the generated on the surface of high temperature as the electrons pass through the sample, the active substances, including sulfur or polysulfide, was

Fig. 7 TEM images of S/U-CN composite after cycling process at different electron irradiation times: **a** 0 s, **b** 5 s, **c** 10 s, and **d** 30 s
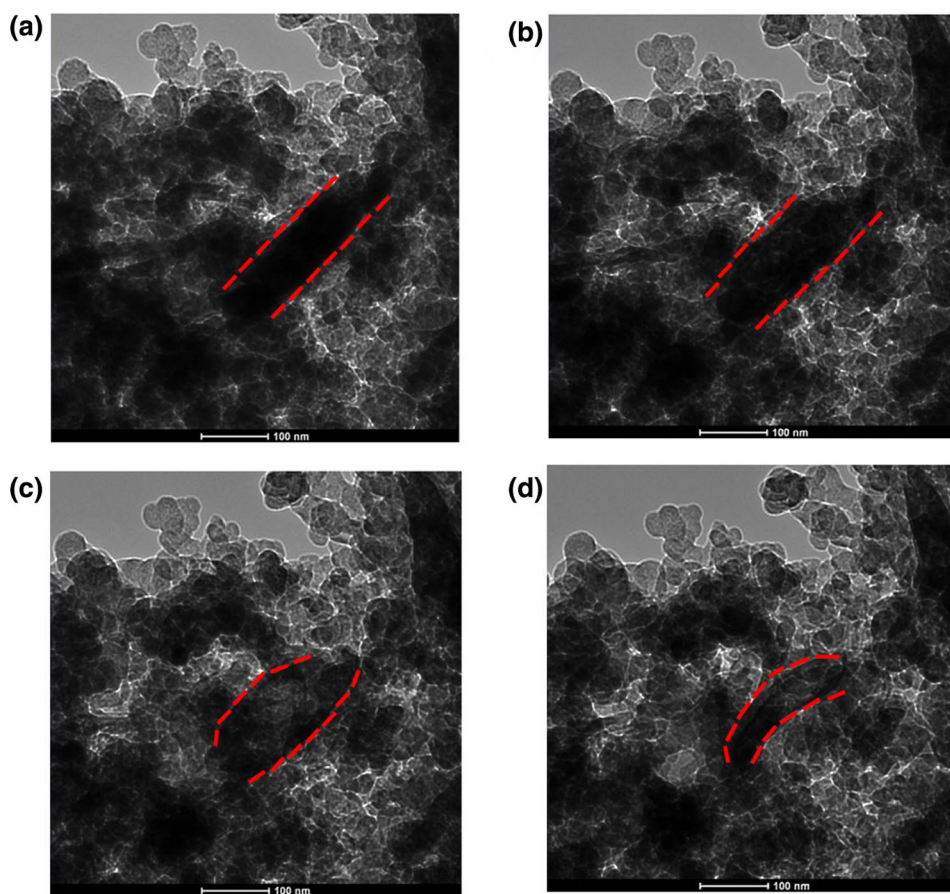
obviously sublimated. A video (shown in supplementary material) exhibited the changing of sublimation process. Figure 7a–d shows several screen shots of abovementioned video at different times, respectively. Obviously, the increase in sulfur or polysulfide on U-CN surface with electron irradiation gradually disappears. Therefore, since electron radiation radiates heat generated on the surface of the sample for a long time, active substances have become sublimated in the testing environment. Meanwhile, the black area changed significantly that only U-CN sheets were still visible, which demonstrated as-prepared U-CN can not only suppress the trapped the polysulfides and increased the utilization of element sulfur by retraining the shuttle effect. These experiment results further certify the prospective program that introducing U-CN used as sulfur matrix can constrain the shuttle effect of LSB, reutilization of the active material and improve the electrochemical behavior of LSB.

4 Conclusion

In summary, g-C_3N_4 samples were prepared via a simple pyrolysis of urea, melamine, thiourea and dicyandiamide under the same procedures, respectively. The as-prepared g-C_3N_4 was used as sulfur matrix in lithium–sulfur batteries. The electrochemical performance of the g-C_3N_4 was found to be influenced more by the pore size distribution and pore volume. The urea-derived g-C_3N_4 (U-CN) exhibited the highest specific area, largest pore volume and crinkly paper-folded thinner sheets. Compared with pure sulfur cathode, the S/U-CN composite improved electrochemical properties, which can not only provide more active sites during charge–discharge process, but also be beneficial the immersion of electrolyte in cathode. Our research results could provide significant insights into appropriate choice of precursors for g-C_3N_4 synthesis as sulfur matrix in lithium–sulfur batteries.

References

1. G. Jeong, Y.U. Kim, H. Kim, Y.J. Kim, H.J. Sohn, Prospective materials and applications for Li secondary batteries. Energy Environ. Sci **4**, 1986–2002 (2011)

2. K.A. Kurilenko, O.A. Shlyakhtin, O.A. Brylev, D.I. Petukhov, A.V. Garshev, Effect of nanostructured carbon coatings on the electrochemical performance of $Li_{1.4}Ni_{0.5}Mn_{0.5}O_{2+x}$-based cathode materials. Beilstein J. Nanothechnol. **7**, 1960–1970 (2016)

3. J.Q. Li, C. Han, M.X. Jing, H. Yang, X.Q. Shen, S.B. Qin, Flake-like oxygen-deficient lithium vanadium oxides as a high ionic and electronic conductive cathode materials for high power Li-ion battery. Appl. Phys. A **124**, 450 (2018)

4. B.Y. Sun, Q.L. Liu, W.S. Chen, N. Wang, J.J. Gu, W. Zhang, H.L. Su, D. Zhang, Micron-sized encapsulated-type MoS_2/C hybrid particles with an effective confinement effect for improving the cycling performance of LIB anodes. J. Mater. Chem. A **6**, 6289–6298 (2018)

5. N. Wang, Q.L. Liu, B.Y. Sun, J.J. Gu, B.X. Yu, W. Zhang, D. Zhang, N-doped catalytic graphitized hard carbon for high-performance lithium/sodium-ion batteries. Sci. Rep. UK **8**, 9934 (2018)

6. D.M. Kang, Q.L. Liu, M. Chen, J.J. Gu, D. Zhang, Spontaneous cross-linking for fabrication of nanohybrids embedded with size-controllable particles. ACS Nano **10**, 889–898 (2016)

7. R. Zhuang, S. Yao, M. Jing, X. Shen, T. Li, S. Qin, Synthesis and characterization of electrospun molybdenum dioxide–carbon nanofibers as sulfur matrix additives for rechargeable lithium–sulfur battery applications. Beilstein J. Nanothechnol. **9**, 262–270 (2018)

8. J. Liu, W. Li, L. Duan, X. Li, L. Ji, Z. Geng, K. Huang, L. Lu, A graphene-like oxygenated carbon nitride material for improved cycle-life lithium/sulfur batteries. Nano Lett. **15**, 5137–5142 (2015)

9. H. Tang, S. Yao, M. Jing, X. Wu, J. Hou, X. Qian, D. Rao, Q. Shen, Nickel fibers/sulfur composites cathode with enhanced electrochemical performance for rechargeable lithium-sulfur batteries. Electrochim. Acta **176**, 442–447 (2015)

10. H.L. Lee, Z. Sofer, V. Mazanek, J. Luxa, C.K. Chua, M. Pumera, Graphitic carbon nitride: effects of various precursors on the structural, morphological and electrochemical sensing properties. Appl. Mater. Today **8**, 150–162 (2017)

11. L. Ma, K.E. Hendrickson, S. Wei, L.A. Archer, Nanomaterials: Science and applications in the lithium–sulfur battery. Nano Today **10**, 315–338 (2015)

12. Q. Pang, X. Liang, C.Y. Kwok, L.F. Nazar, Advances in lithium–sulfur batteries based on multifunctional cathodes and electrolytes. Nat. Energy **1**, 16132 (2016)

13. J.L. Hou, S.S. Yao, X. Wu, M.X. Jing, D.W. Rao, X.Q. Shen, X.M. Xi, K.S. Xiao, Fabrication and characterization of non-woven carbon nanofibers as functional interlayer for rechargeable lithium sulfur battery. J. Nanosci. Nanotechnol. **17**, 1857–1862 (2017)

14. M. Barghamadi, A.S. Best, A.I. Bhatt, A.F. Hollenkamp, P.J. Mahon, M. Musameh, T. Rjither, Effect of $LiNO_3$ additive and pyrrolidinium ionic liquid on the solid electrolyte interphase in the lithium–sulfur battery. J. Power Sources **295**, 212–220 (2015)

15. H.J. Peng, D.W. Wang, J.Q. Huang, X.B. Cheng, Z. Yuan, F. Wei, Q. Zhang, Janus separator of polypropylene-supported cellular graphene framework for sulfur cathodes with high utilization in lithium–sulfur batteries. Adv. Sci. **3**, 1500268 (2016)

16. Y.J. Li, J.M. Fan, M.S. Zheng, Q.F. Dong, A novel synergistic composite with multi-functional effects for high-performance Li–S batteries. Energy Environ. Sci. **9**, 1998–2004 (2016)

17. X. Liang, C. Hart, Q. Pang, A. Garsuch, T. Weiss, L.F. Nazar, A highly efficient polysulfide mediator for lithium–sulfur batteries. Nat. Commun. **6**, 5682 (2015)

18. X.Q. Zhang, B. He, W.C. Li, A.H. Lu, Hollow carbon nanofibers with dynamic adjustable pore sizes and closed ends as hosts for high-rate lithium-sulfur battery cathodes. Nano Res. **11**(3), 1238–1246 (2018)

19. H. Li, X. Yang, X. Wang, M. Liu, F. Ye, J. Wang, Y. Zhang, Dense integration of graphene and sulfur through the soft approach for compact lithium/sulfur battery cathode. Nano Energy **12**, 468–475 (2015)

20. J. Song, M.L. Gordin, T. Xu, S. Chen, Z. Yu, H. Sohn, D. Wang, Strong lithium polysulfide chemisorption on electroactive sites of nitrogen-doped carbon composites for high-performance lithium–sulfur battery cathodes. Angew. Chem. Int. Ed. **54**, 4325–4329 (2015)

21. J.Q. Huang, Z.L. Xu, S. Abouali, M.A. Garakani, J.K. Kim, Porous graphene oxide/carbon nanotube hybrid films as interlayer for lithium-sulfur batteries. Carbon **99**, 624–632 (2016)

22. S.S. Yao, S.K. Xue, Y.J. Zhang, X.Q. Shen, X.Y. Qian, T.B. Li, K.S. Xiao, S.B. Qin, J. Xiang, Synthesis, characterization, and electrochemical performance of spherical nanostructure of Magnéli phase Ti_4O_7. J. Mater. Sci. Mater. Electron. **28**, 7264–7270 (2017)

23. K. Chen, Z. Sun, R. Fang, Y. Shi, H.M. Cheng, F. Li, Metal–organic frameworks (MOFs)-derived nitrogen-doped porous carbon anchored on graphene with multifunctional effects for lithium-sulfur batteries. Adv. Funct. Mater. **2018**, 1707592 (2018)

24. M. Zhang, C. Yu, C. Zhao, X. Song, X. Han, S. Liu, J. Qiu, Cobalt-embedded nitrogen-doped hollow carbon nanorods for synergistically immobilizing the discharge products in lithium–sulfur battery. Energy Storage Mater. **5**, 223–229 (2016)

25. Y. Qiu, W. Li, W. Zhao, G. Li, Y. Hou, M. Liu, S. Yang, High-rate, ultralong cycle-life lithium/sulfur batteries enabled by nitrogen-doped graphene. Nano Lett. **14**, 4821–4827 (2014)

26. X. Bu, J. Li, S. Yang, J. Sun, Y. Deng, Y. Yang, G. Ding, Surface modification of C_3N_4 through oxygen-plasma treatment: a simple way toward excellent hydrophilicity. ACS Appl. Mater. Interfaces **8**, 31419–31425 (2016)

27. G. Zhang, C. Huang, X. Wang, Dispersing molecular cobalt in graphitic carbon nitride frameworks for photocatalytic water oxidation. Small **11**, 1215–1221 (2015)

28. Z. Zhang, K. Leinenweber, M. Bauer, L.A. Garvie, P.F. McMillan, G.H. Wolf, High-pressure bulk synthesis of crystalline $C_6N_9H_3 \cdot HCl$: a novel C_3N_4 graphitic derivative. J. Am. Chem. **123**, 7788–7796 (2001)

29. H. Xu, J. Yan, Y. Xu, Y. Song, H. Li, J. Xia, H. Wan, Novel visible-light-driven AgX/graphite-like C_3N_4 (X = Br, I) hybrid materials with synergistic photocatalytic activity. Appl. Catal B Environ. **129**, 182–193 (2013)

30. P.K. Chuang, K.H. Wu, T.F. Yeh, H. Teng, Extending the π-conjugation of g-C_3N_4 by incorporating aromatic carbon for photocatalytic H_2 evolution from aqueous solution. ACS Sustain. Chem. Eng. **227**, 153–160 (2016)

31. L. Stagi, D. Chiriu, C.M. Carbonaro, R. Corpino, P.C. Ricci, Structural and optical properties of carbon nitride polymorphs. Diam. Relat. Mater. **68**, 84–92 (2016)

32. S.S. Yao, S.K. Xue, S. H.Peng, M.X. Jing, X.Y. Qian, X.Q. Shen, T.B. Li, Y.H. Wang, Synthesis of graphitic carbon nitride at different thermal-pyrolysis temperature of urea and it application in lithium sulfur batteries. J. Mater. Sci. Mater. Electron. **29**, 17921–17930 (2018)

33. Z. Zeng, H. Yu, X. Quan, S. Chen, S. Zhang, Structuring phase junction between tri-s-triazine and triazine crystalline C_3N_4 for efficient photocatalytic hydrogen evolution. Appl. Catal. B Environ. **227**, 153–160 (2018)

34. M. Zhou, Z. Hou, L. Zhang, Y. Liu, Q. Gao, X. Chen, n/n junctioned g-C_3N_4 for enhanced photocatalytic H_2 generation. Sustain. Energy Fuels **1**, 317–323 (2017)

35. Y. Li, Q.L. Liu, D.M. Kang, J.J. Gu, W. Zhang, D. Zhang, Free-drying assisted synthesis of hierarchical porous carbons for high-performance supercapacitors. J. Mater. Chem. A **3**, 21016–21022 (2015)

36. S. Panneri, P. Ganguly, B.N. Nair, A.A.P. Mohamed, K.G.K. Warrier, U.N.S. Hareesh, Role of precursors on the photophysical properties of carbon nitride and its application for antibiotic degradation. Environ. Sci. Pollut. R **24**, 8609–8618 (2017)

37. F.Y. Zhou, Q.L. Liu, D.M. Kang, J.J. Gu, W. Zhang, D. Zhang, A 3D hierarchical hybrid nanostructure of carbon nanotubes and activated carbon for high-performance supercapacitors. J. Mater. Chem. A **2**, 3505–3512 (2014)

38. J. Wang, J. Huang, H. Xie, A. Qu, Synthesis of g-C_3N_4/TiO_2 with enhanced photocatalytic activity for H_2 evolution by a simple method. Int. J. Hydrog. **39**, 6354–6363 (2014)

39. X. Tao, J. Wang, C. Liu, H. Yao, G. Zheng, C. Zu, Balancing surface adsorption and diffusion of lithium-polysulfides on nonconductive oxides for lithium–sulfur battery design. Nat. Commun. **7**, 11203 (2016)

40. B. Li, C. Han, Y.B. He, C. Yang, H. Du, Q.H. Yang, F. Kang, Facile synthesis of $Li_4Ti_5O_{12}$/C composite with super rate performance. Energy Environ. Sci. **5**, 9595–9602 (2012)

41. K. Luan, S. Yao, Y. Zhang, R. Zhuang, J. Xiang, X. Shen, S. Qin, Poly (3, 4-ethyleendioxythiophene) coated titanium dioxide nanoparticles in situ synthesis and their application for rechargeable lithium sulfur batteries. Electrochim. Acta **252**, 461–469 (2017)

42. P. Mei, X.L. Wu, H. Xie, L. Sun, Y. Zeng, J. Zhang, C. Yao, LiV_3O_8 nanorods as cathode materials for high-power and long-life rechargeable lithium-ion batteries. RSC Adv. **4**, 25494–25501 (2014)

43. H. Tang, S. Yao, S. Xue, M. Liu, L. Chen, M. Jing, X. Shen, T. Li, K. Xiao, S. Qin, In-situ synthesis of carbon@Ti_4O_7 non-woven fabric as a multifunctional interlayer for excellent lithium sulfur battery. Electrochim. Acta **263**, 158–167 (2018)